

# Effect of $\text{La}_2\text{O}_3$ Addition on Microstructure and Tribological Performance of Laser Cladded Ni-WC Coating on S136 Steel

Xu Yongfu<sup>1</sup> · Kong Dejun<sup>1</sup> 

Received: 22 January 2022 / Accepted: 6 February 2022 / Published online: 18 March 2022  
© The Indian Institute of Metals - IIM 2022

**Abstract**  $\text{La}_2\text{O}_3$  reinforced Ni-WC coatings were prepared on S136 steel by laser cladding technique. The microstructure and phase of obtained coatings were analyzed using an ultra depth of field microscope and X-ray diffraction, respectively. The effect of  $\text{La}_2\text{O}_3$  mass fraction on the microstructure and friction-wear performance of Ni-WC coating was investigated. The results show that the coefficients of frictions (COFs) of Ni-WC-3% $\text{La}_2\text{O}_3$ , - 6% $\text{La}_2\text{O}_3$  and - 9% $\text{La}_2\text{O}_3$  are decreased by 26.7%, 34.8% and 22.4% than that of substrate, in which the COF of Ni-WC-6% $\text{La}_2\text{O}_3$  is the smallest among the three kinds of coatings. The wear rates of substrate and Ni-WC-3% $\text{La}_2\text{O}_3$ , - 6% $\text{La}_2\text{O}_3$  and - 9% $\text{La}_2\text{O}_3$  coatings are 640.81, 344.78, 402.63, 422.38  $\mu\text{m}^3 \cdot \text{s}^{-1} \cdot \text{N}^{-1}$ , respectively, which increase with the increase of  $\text{La}_2\text{O}_3$  mass fraction. The wear mechanisms of Ni-WC coatings with the 3%, 6% and 9% $\text{La}_2\text{O}_3$  mass fractions are adhesive wear + oxidation wear, adhesive wear, and adhesive wear + oxidation wear, respectively, showing that the appropriate  $\text{La}_2\text{O}_3$  mass fraction plays the role of wear resistance of Ni-WC- $\text{La}_2\text{O}_3$  coatings.

**Keywords** Laser cladding (LC) · Ni-WC coating ·  $\text{La}_2\text{O}_3$  mass fraction · Coefficient of frictions (COF) · Wear mechanism

## 1 Introduction

Traditional technique of thermal spraying is often used to fabricate surface coatings, however, no metallurgical bonding is formed between the sprayed coatings and the substrates, which affects their use performance. As an advanced coating technology, laser cladding (LC) may form a good metallurgical bonding due to the effect of melting pool at the coating-substrate interface [1]. LC has the many advantages, such as low dilution rate, metallurgical bonding, high hardness, wear resistance and corrosion resistance [2], which are widely used to fabricate the coatings on key parts [3].

Hard-faced coatings of Fe-, Ni- and Co-based alloys have high wear resistance [4], which has broad application prospects in surface engineering [5]. Among them, Ni-based alloy coatings are widely used to improve the quality of rolling mills, tools, rollers, etc., in which Ni is the main element to provide ductility and corrosion resistance; Cr has high wear resistance and corrosion resistance; B enhances wear resistance; and Si reduces the melting point of Ni-based alloy coatings.

In order to further expand the use fields of Ni-based alloy coatings, scholars have conducted extensive researches on tungsten carbide (WC) to strengthen Ni-based coatings [6]. Due to the large difference in thermal expansion coefficients of WCs and Ni-based alloy coating, excessive stress often occurs at the interface of Ni-WC coatings, resulting in cracks in the coatings [7]. Another kind of elements that can enhance the mechanical property of carbides is rare earth elements, which form a flat cross between hardness and toughness, and improve the hardness and oxidation resistance of coatings [8]. Sharma et al. [4] found that adding 1.2%  $\text{La}_2\text{O}_3$  to NiCrBSi coating refined the grain and caused the element distribution uniform, and

✉ Kong Dejun  
kong-dejun@163.com

<sup>1</sup> School of Mechanical Engineering, Changzhou University, Changzhou 213164, People's Republic of China

the hardness of NiCrBSi-1.2%  $\text{La}_2\text{O}_3$  coating increased by 22% and the wear resistance increased by 25% compared with NiCrBSi coating. Li et al. [3] also found that the addition of 0.6%  $\text{La}_2\text{O}_3$  to the Ni-based coating was conducive to the formation of crack-free coating and the refinement of microstructure, which improved the corrosion resistance compared with the Ni-based coating.

In this work, Ni-WC coatings with the different  $\text{La}_2\text{O}_3$  mass fractions were prepared on S136 steel by LC. The microstructure, friction coefficient and wear rate of Ni-based-WC coatings with the different  $\text{La}_2\text{O}_3$  mass fractions were investigated, and the wear mechanism was also discussed in detail.

## 2 Experimental

### 2.1 Coating Preparations

S136 steel with the hardness of 510 HV was selected as the substrate, and its chemical composition (wt, %) was C 0.40, Si 0.8, Mn 0.50, Cr 13.5, V 0.20, Mo 0.60, S 0.03 and the rest was Fe. The parameters of heat treatment were shown as follows: preheating temperature of 800 °C; quenching temperature of 1030 °C; and tempering temperature of 250 °C for 2 h. The laser cladding material was 30%Ni coated 70%WC (Ni-WC) powder with the particle size of 45–75  $\mu\text{m}$  (Chengdu Huayin Powder Technology Limited Company, China), and the  $\text{La}_2\text{O}_3$  powder (Hebei Yili Metallurgical Materials Limited Company, China) was added to the Ni-WC powder with the respective mass fractions of 3%, 6% and 9%, which was mixed on a QM-3SP041 planetary miller (Nanjing University Instrument Factory, China) with the rotating speed of 500 r/min for 2 h.

The LC test was carried out on an RFL-C3300 type optical fiber-coupled laser system (Changzhou Weilai Intelligent Technology Co., Ltd), and the sketch of LC

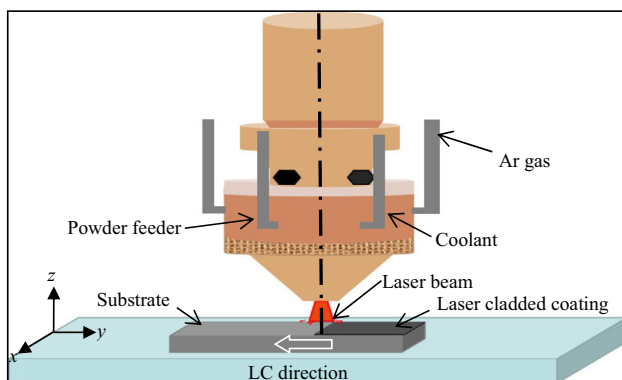


**Fig. 1** Sketch of LC process for reinforced Ni-WC- $\text{La}_2\text{O}_3$  coatings

process is shown in Fig. 1, in which the laser head moving, powder feeding and working feed directions were  $x$ ,  $y$  and  $z$  axes, respectively. After the several pre-tests, the LC parameters were determined as follows: wavelength of 1064 nm; fiber diameter of 10  $\mu\text{m}$ ; laser power of 1000 W; spot diameter of 4 mm; scanning rate of 3 mm/s; and powder feeding rate of 85 g/min; distance between the laser head and the substrate of 10 mm; and shrouding gas of Ar.

### 2.2 Characterization Methods

After the LC test was ended, the coating sample was cut to the dimension of 15 × 15 × 5 mm, and the coating surface and cross section were polished with SiC abrasive paper on a metallographic polishing machine. The microstructure of obtained coating was analyzed using a VHX-700 type ultra depth of field microscope (UDFM) (Keyence Co., Ltd., Japan), which was optical microscope. The phase composition was analyzed using a D/max2500 type PC X-ray diffraction (XRD) (Rigaku Co., Ltd., Japan), in which Cu-target and Ka-radiation were used for the measurement.

### 2.3 Friction-Wear Test

The friction-wear test was conducted on a CFT-1 type friction tester (Lanzhou Zhongke Kaihua Technology Development Co., Ltd, China) at normal temperature, in which three-time friction tests were carried out on each sample, and the average values were presented as the experimental results. The test parameters were tribo-pair of  $\text{Si}_3\text{N}_4$  ball with the diameter of 4 mm, load of 8 N, speed of 3.3 Hz, and sliding length of 5 mm.

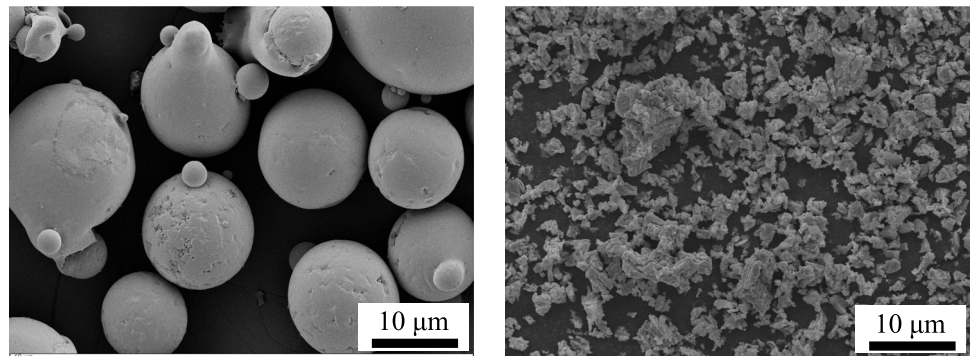
After the wear test was finished, the depth and width of wear marks were analyzed using an UDFM, and the worn morphologies and chemical elements were analyzed using a JSM-6360LA type scanning electron microscope (SEM) and energy-dispersive spectrometer (EDS), respectively, and the wear model was established to analyze the effect of  $\text{La}_2\text{O}_3$  mass fractions on the friction-wear performance of Ni-WC coating.

## 3 Results Analysis and Discussion

### 3.1 Morphologies and XRD Analysis of Powders

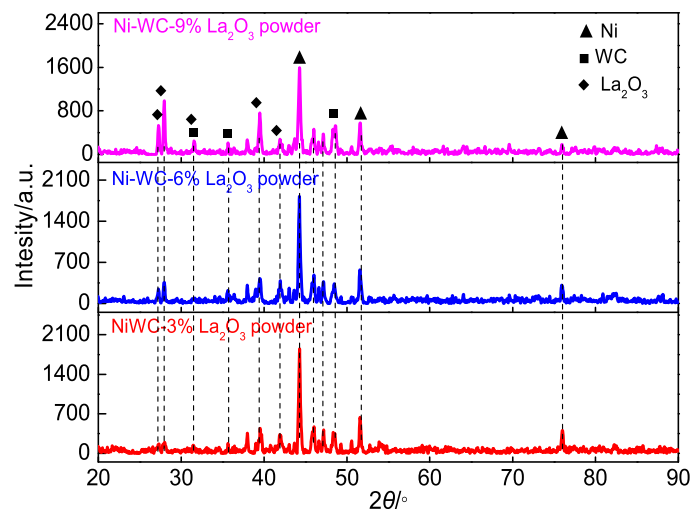
Figure 2a shows the morphology of Ni-WC powder. The WC was of spherical shape, which had good fluidity. Figure 2b shows the morphology of  $\text{La}_2\text{O}_3$  powder. The powder was of irregular shape, which was easily combined with the Ni-WC powder. Figure 2c shows the XRD results

**Fig. 2** Morphologies and XRD analysis of Ni-WC and La<sub>2</sub>O<sub>3</sub> powders



(a) Ni-WC powder

(b) La<sub>2</sub>O<sub>3</sub> powder



(c) XRD patterns

of Ni-WC and La<sub>2</sub>O<sub>3</sub> mixed powders. The powders were mainly composed of Ni, WC and La<sub>2</sub>O<sub>3</sub> phases, and the addition of La<sub>2</sub>O<sub>3</sub> did not change the peaks, but only affected the peak heights.

### 3.2 Microstructure of Coatings

Figure 3a shows the microstructure of Ni-WC-3%La<sub>2</sub>O<sub>3</sub> coating surface and cross section. The dendritic structure was sparse shaped with the different lengths, which were surrounded by the disordered metallographic structure. The coating cross section had no obvious cracks and holes, and the WC was uniformly distributed on its cross section.

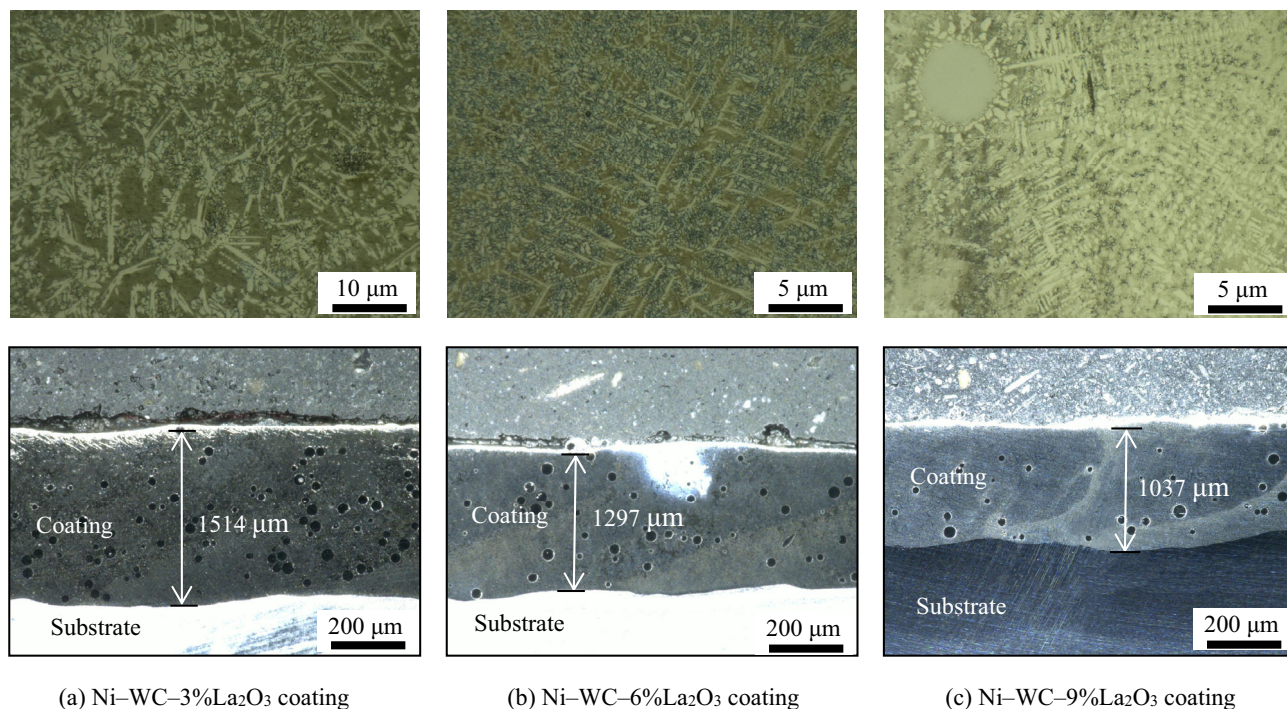
Figure 3b shows the microstructure of Ni-WC-6%La<sub>2</sub>O<sub>3</sub> coating surface and cross section. The long dendritics were closely connected to each other, in which the addition of La<sub>2</sub>O<sub>3</sub> significantly refined the dendrite structure [9]. The coating cross section had no obvious hole defects, and the WC was scattered on its cross section.

Figure 3c shows the microstructure of Ni-based-WC-9%La<sub>2</sub>O<sub>3</sub> coating surface. The coating also presented long dendritic crystal shape, in which the dendritic structure was evenly distributed on both sides of trunks. There were no obvious cracks and holes, and the fusion line between the coating and the substrate was wavy, which was because the high density of laser beam led to the irregular shape [10]. In this case, the metallurgical bonding was formed at the coating interface due to the melting pool effect of laser, which enhanced the bonding strength between the coating and the substrate [11].

Figure 4 shows the XRD results of Ni-WC-La<sub>2</sub>O<sub>3</sub> coatings. The coatings were composed of FeNi<sub>3</sub>, Fe<sub>3</sub>C, W<sub>2</sub>C and La<sub>2</sub>O<sub>3</sub> phases, showing that the WC was decarbonized to produce a small amount of W<sub>2</sub>C.

### 3.3 Friction-Wear Performances

The COFs of Ni-WC-La<sub>2</sub>O<sub>3</sub> coatings vs wear time was obtained by the friction tester, as shown in Fig. 5a. The



**Fig. 3** Microstructure of Ni-WC-La<sub>2</sub>O<sub>3</sub> coating surfaces cross sections with different La<sub>2</sub>O<sub>3</sub> mass fractions

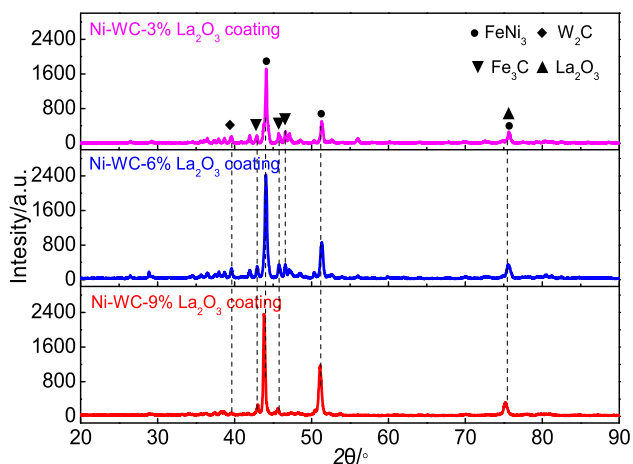


**Fig. 4** XRD analysis of Ni-WC-La<sub>2</sub>O<sub>3</sub> coatings with different La<sub>2</sub>O<sub>3</sub> mass fractions

average COFs of substrate and Ni-WC coatings with the mass fractions of 3%La<sub>2</sub>O<sub>3</sub>, 6%La<sub>2</sub>O<sub>3</sub> and 9%La<sub>2</sub>O<sub>3</sub> were 0.792, 0.580, 0.516, and 0.614, respectively. Among them, the friction reduction effect of 6% La<sub>2</sub>O<sub>3</sub> was the best, and that of 9%La<sub>2</sub>O<sub>3</sub> was the worst. The WC effectively reduced the COF of Ni-WC-La<sub>2</sub>O<sub>3</sub> coating due to its high hardness [12], and the addition of La<sub>2</sub>O<sub>3</sub> further reduced its COFs, showing that the appropriate La<sub>2</sub>O<sub>3</sub> mass fraction played a role of friction reduction.

Figure 5b shows the outlines of worn tracks on the Ni-WC-La<sub>2</sub>O<sub>3</sub> coatings with the different La<sub>2</sub>O<sub>3</sub> mass

fractions. The wear volumes of substrate and Ni-WC-3%La<sub>2</sub>O<sub>3</sub>, -6%La<sub>2</sub>O<sub>3</sub> and -9%La<sub>2</sub>O<sub>3</sub> coatings were  $9.22 \times 10^6$ ,  $4.96 \times 10^6$ ,  $5.79 \times 10^6$ , and  $6.08 \times 10^6 \mu\text{m}^3$ , respectively, and the corresponding wear rates were 640.81, 344.78, 402.636, and  $422.38 \mu\text{m}^3 \cdot \text{s}^{-1} \cdot \text{N}^{-1}$ , respectively, as shown in Fig. 5c. The results showed that the wear rates of La<sub>2</sub>O<sub>3</sub> reinforced Ni-WC coatings were lower than that of substrate, but excessive La<sub>2</sub>O<sub>3</sub> led to the La<sub>2</sub>O<sub>3</sub> agglomeration and wear resistance declining [13].

### 3.4 Morphologies and EDS Analysis of Worn Tracks

Figure 6a shows the morphology and EDS analysis of worn track on the substrate. There was little debris on the worn track, which continued to wear the worn track under the action of normal load. The debris changed the wear mechanism of two-body to that of three-body, resulting in abrasive wear [14]. The EDS analysis at the A point showed that the worn track was composed of Fe, Cr, C, O and Si, and the oxides and carbides of Fe and Cr mainly existed on the worn track. It was indicated that the substrate underwent oxidative wear in the friction process, and the oxide was formed on the worn track, which played a protective role.

Figure 6b shows the morphology and EDS analysis of worn track on the Ni-WC-3%La<sub>2</sub>O<sub>3</sub> coating. The adhesive wear occurred under the action of normal load, and the fragments of abrasive wear rubbed back and forth on the

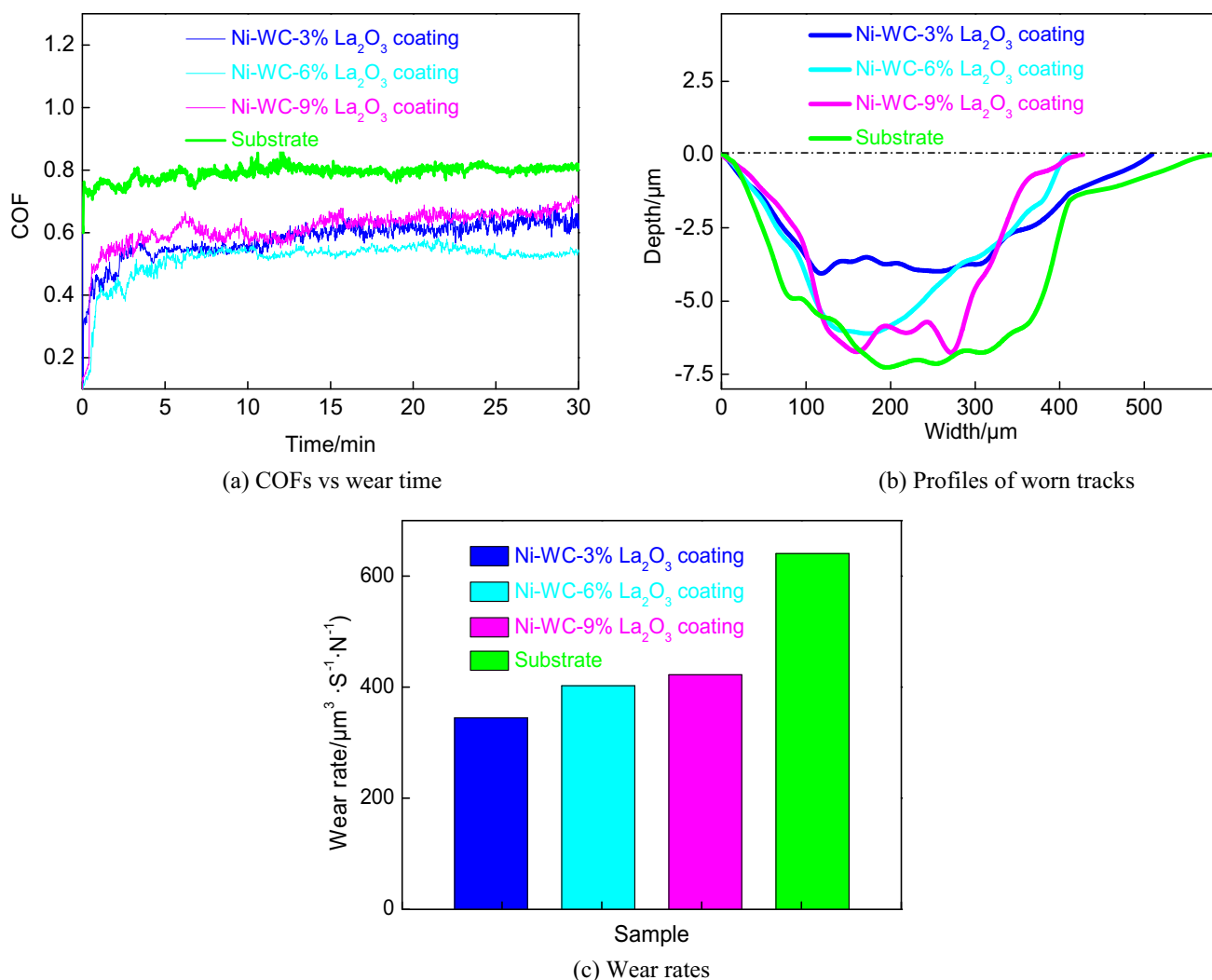
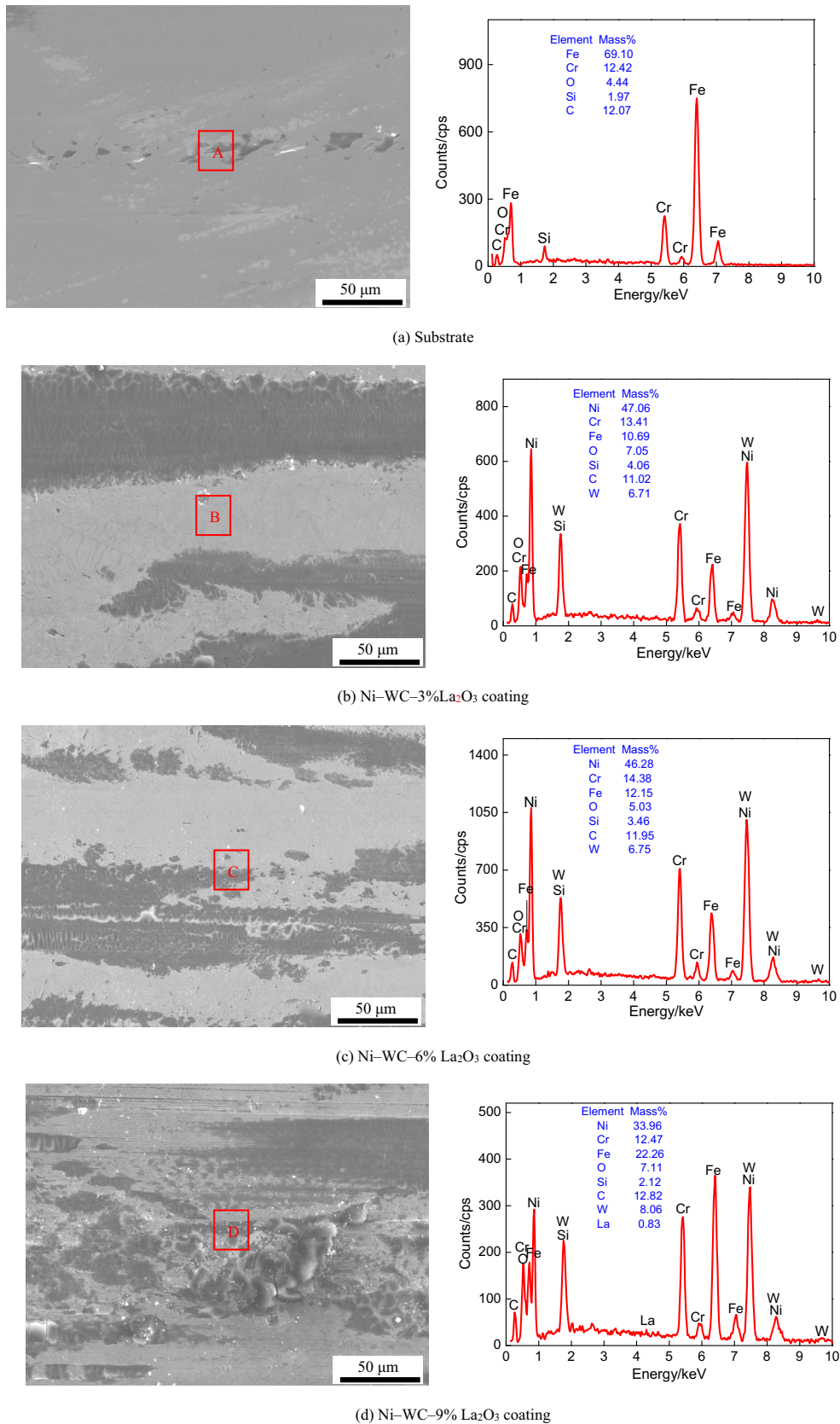


**Fig. 5** COFs versus wear time, profiles of worn tracks and wear rates of Ni-WC-La<sub>2</sub>O<sub>3</sub> coatings with different La<sub>2</sub>O<sub>3</sub> mass fractions

worn track, leaving obvious furrows. The EDS analysis results at the B point showed that the worn track was composed of W, C, Ni, Cr, Fe, O and Si. The O content on the worn track came from the La<sub>2</sub>O<sub>3</sub> and oxides, indicating that the worn track underwent oxidation wear. The Ni-WC coating with the high hardness resisted the cutting effect of normal load, and the wear track was relatively smooth. Therefore, the wear mechanism was abrasive wear and oxidation wear [15].

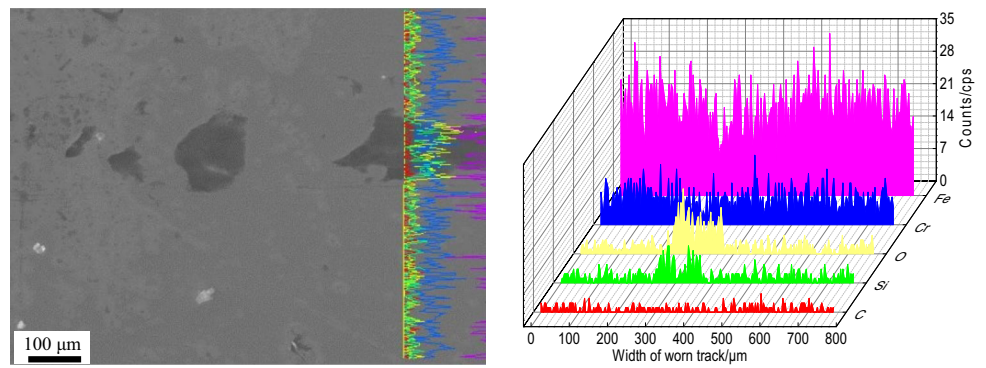
Figure 6c shows the morphology and EDS analysis of worn track of Ni-WC-6%La<sub>2</sub>O<sub>3</sub> coating. There were obvious adhesive traces, brittle spalling and gullies, which was the feature of adhesive wear. The EDS analysis at the C point showed that the coating was composed of C, O, W, Fe, Ni, Cr and Si. The oxide presence indicated that the oxidation wear occurred on the worn track. Therefore, the wear mechanism was mainly adhesive wear, accompanied by a small amount of oxidation wear.

Figure 6d shows the worn track morphology and EDS analysis of Ni-WC-9%La<sub>2</sub>O<sub>3</sub> coating. There were many abrasives and larger wear debris on the worn track, and some parts of worn track were cracked to form fatigue cracks. This was because, a lot of hard carbides were formed on the worn track, which enhanced the coating brittleness. In this case, the fatigue cracks were easily propagated on the worn track surface, which expanded further until the surface layer was stripped and peeled off from the substrate. In this case, the wear fragments from edge cracks led to the increase of COFs [16]. The EDS analysis result at the D point showed that the worn track was composed of C, W, Fe, Ni, Cr, Si, O and La. The presence of La and O indicated that the coating was not worn through. The increases of W and C also indicated that the La<sub>2</sub>O<sub>3</sub> inhibited the peeling of WC particles on the worn track [17]. Compared with the images in Fig. 6b and c, the obvious changes in Fig. 6d were the decrease of Ni

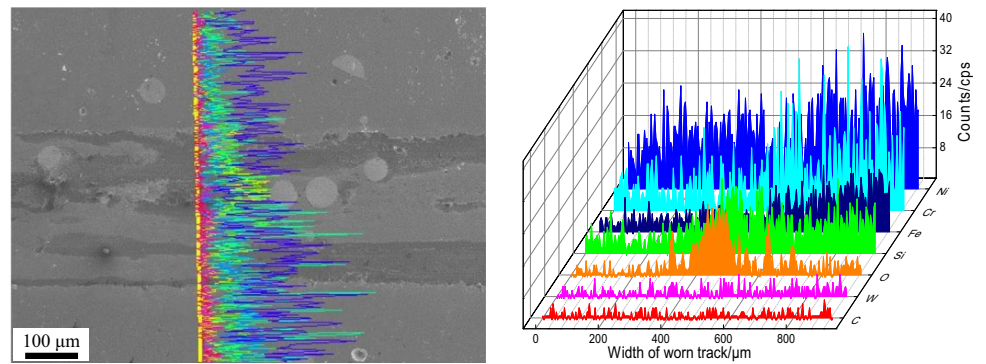


**Fig. 6** Morphologies and EDS analysis of worn tracks on substrate and Ni-WC-La<sub>2</sub>O<sub>3</sub> coatings with different La<sub>2</sub>O<sub>3</sub> mass fractions

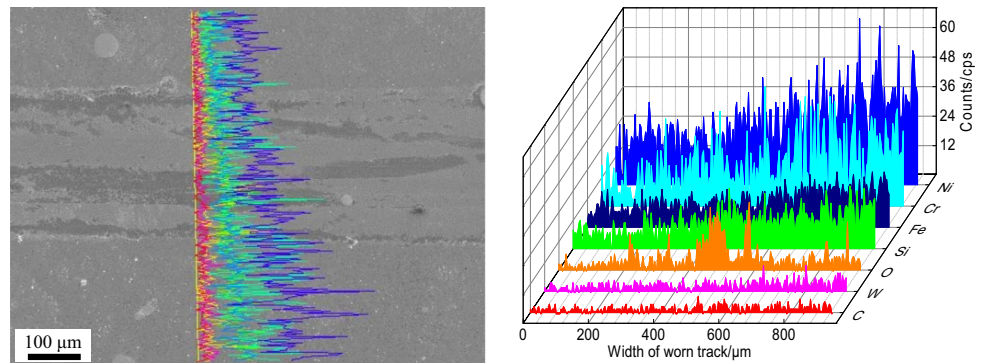
**Fig. 7** Line scan analysis of worn track on Ni-WC-La<sub>2</sub>O<sub>3</sub> coatings with different La<sub>2</sub>O<sub>3</sub> mass fractions



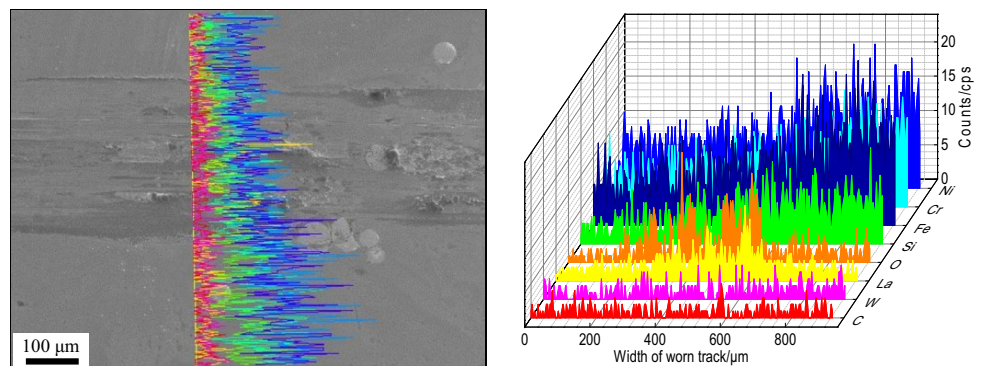
(a) On substrate



(b) On Ni-WC-3% La<sub>2</sub>O<sub>3</sub> coating



(c) On Ni-WC-6% La<sub>2</sub>O<sub>3</sub> coating



(d) Ni-WC-9% La<sub>2</sub>O<sub>3</sub> coating

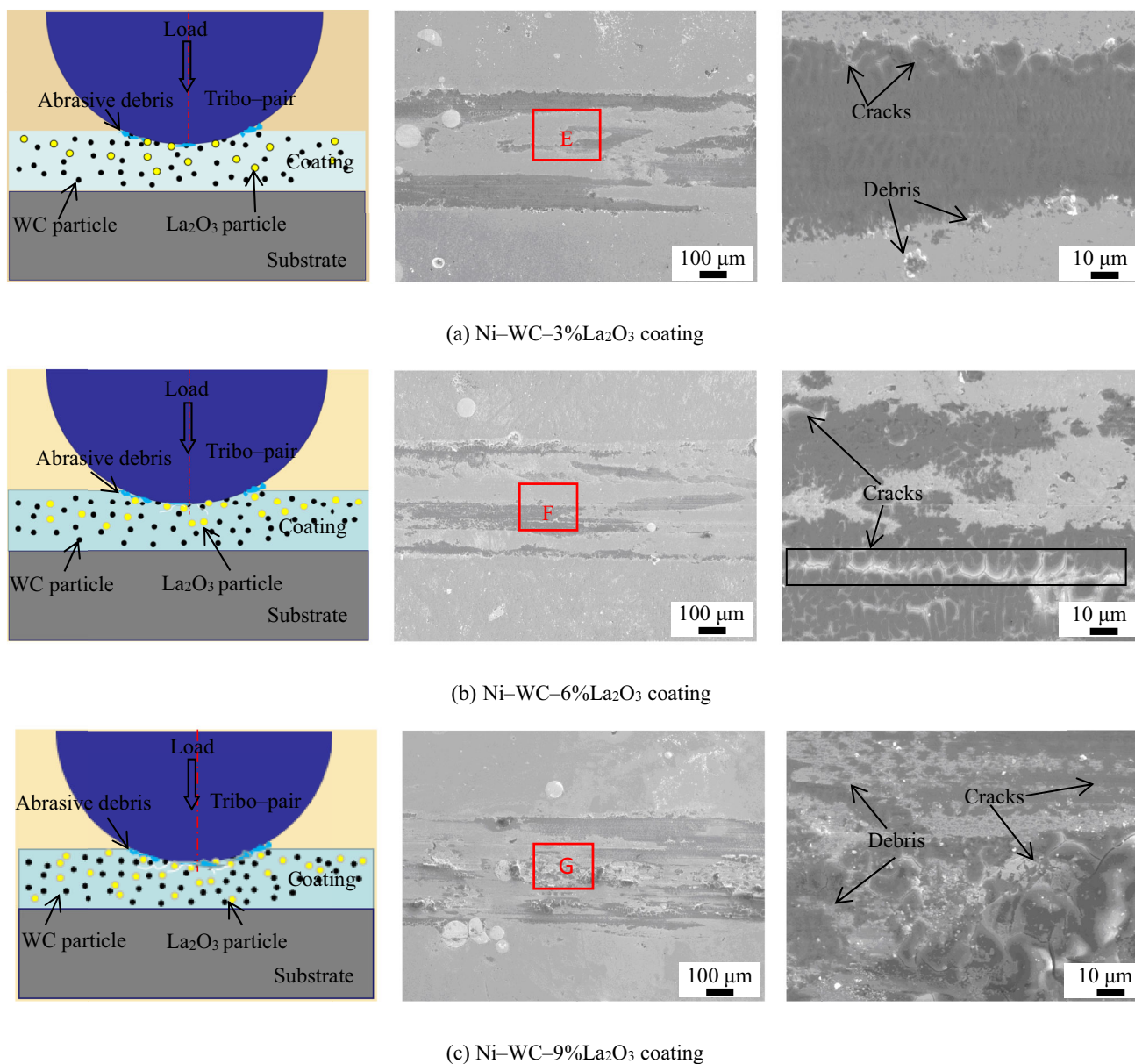


**Fig. 8** Wear mechanisms of Ni-WC-La<sub>2</sub>O<sub>3</sub> coatings with different La<sub>2</sub>O<sub>3</sub> mass fractions

and the increase of Fe due to the falling off of debris in the friction process.

### 3.5 EDS Scan Analysis of Worn Tracks

Figure 7a shows the line scanning analysis of worn track on the substrate, in which the Fe, Cr, C, O and Si were detected on the worn track. Compared with the substrate, the O content was increased significantly due to the oxidation wear by the friction heat [18].

Figure 7b shows the line scanning analysis of worn track on the Ni-WC-3% La<sub>2</sub>O<sub>3</sub> coating. The W, C, Fe, Ni, Cr, O and Si were detected on the worn track, in which the

worn track also contained other oxides. The un-melted WC was dispersed and strengthened, which acted as a high hardness skeleton to reduce the wear rate to a certain extent [19].

Figure 7c shows the line scanning analysis of worn track on the Ni-WC-6% La<sub>2</sub>O<sub>3</sub> coating. The Ni, Cr, Fe, W, C, O, and Si were detected on the worn track, in which the W and C were evenly distributed on the worn track. The O existence easily produced adhesive wear, and a small amount of oxide fragments also appeared on the worn track, indicating that the wear mechanism was adhesive wear, accompanied with oxidation wear.

Figure 7d shows the line scanning analysis of worn track on the Ni-WC-9%La<sub>2</sub>O<sub>3</sub> coating. The protruding debris was clearly found on the worn track, which was the feature of fatigue wear. The debris form was carried out from friction continuation to secondary friction on the worn track. The Ni, Cr, Fe, W, C, Si, La and O were detected on the worn track, among them, the La and O came from the La<sub>2</sub>O<sub>3</sub>, indicating that the wear mainly occurred on the coating. The Ni was greatly reduced compared with those in Fig. 7b and c; while the Fe was the opposite in Fig. 7d, which was caused by debris spalling of fatigue wear. The Fe oxides were readily detached from the surface despite continuous formation, and the spalling of Fe oxides generated the fresh surface. The subsequent re-oxidation of debris and detaching of Fe oxides were bound in the friction process due to the abrasion wear [20].

### 3.6 Wear Mechanism

Figure 8a shows the wear model of Ni-WC-3%La<sub>2</sub>O<sub>3</sub>. The sliding mark between the coating and the friction-pair formed the worn track, and a large amount of debris was found, indicating that the wear mechanism was adhesive wear. The enlarged E zone showed that small cracks were found at the edge of the track, which became debris under the action of friction-pair. The detached fragments were not acted as the binder on the worn track, forming an adhesive layer [20]. The results showed that the Ni-WC-3%La<sub>2</sub>O<sub>3</sub> coating had the lowest wear rate, but wear resistance of Ni-WC became worse with the increase of La<sub>2</sub>O<sub>3</sub> mass fraction.

Figure 8b shows the wear model of Ni-WC-6%La<sub>2</sub>O<sub>3</sub> coating. There were no obvious debris accumulations; however, some adhesive parts were found on the worn track, showing that the wear mechanism was adhesive wear. A long crack was found on the worn track, and a large number of small cracks appeared around the long crack, which were the companion cracks. The occurrence of cracks exacerbated the wear progress, leading to fatigue wear on some zones.

Figure 8c shows the wear model of Ni-WC-9%La<sub>2</sub>O<sub>3</sub>. There were many bumps on the worn track, which were clustered together. The amplified G zone indicated that a large number of small white particles were found on the worn track. After the small white particles fell off, the new surface was formed and participated in the friction process. At the same time, the small particles also continued to wear under the action of normal load as an abrasive, turning the two-body wear into a three-body wear [21]. Moreover, many cracks were found on the worn track, which expanded and greatly aggravated the wear loss. As a result, the wear mechanism was adhesive wear and fatigue wear.

## 4 Conclusions

- (1) The Ni-WC-3%La<sub>2</sub>O<sub>3</sub> coating is dendritic structure, and the Ni-WC-6%La<sub>2</sub>O<sub>3</sub> coating is elongated dendritic; while the Ni-WC-9%La<sub>2</sub>O<sub>3</sub> coating presents the long dendritic crystal, in which they are evenly arranged on both sides of the trunk.
- (2) The average COFs of substrate, Ni-based-WC-3% La<sub>2</sub>O<sub>3</sub>, – 6% La<sub>2</sub>O<sub>3</sub> and – 9%La<sub>2</sub>O<sub>3</sub> coatings are 0.792, 0.580, 0.516, and 0.614, respectively. The average COFs first decrease and then increase with the increase of La<sub>2</sub>O<sub>3</sub> mass fraction, which are lower than that of substrate.
- (3) The wear rates of Ni-WC-3%La<sub>2</sub>O<sub>3</sub>, Ni-WC-6%La<sub>2</sub>O<sub>3</sub> and – 9%La<sub>2</sub>O<sub>3</sub> coatings are 344.78, 402.636, 422.38  $\mu\text{m}^3\cdot\text{s}^{-1}\cdot\text{N}^{-1}$ , respectively, which are lower than 640.81  $\mu\text{m}^3\cdot\text{s}^{-1}\cdot\text{N}^{-1}$  of substrate. The results show that the addition of La<sub>2</sub>O<sub>3</sub> has a role of wear resistance, and the appropriate La<sub>2</sub>O<sub>3</sub> mass fraction further reduces the wear rate of Ni-WC-La<sub>2</sub>O<sub>3</sub> coatings.

## References

1. Zhou S F, Zeng X Y, Hu Q W, and Huang Y, *J Appl Surf Sci* **255** (2008) 1646. <https://doi.org/10.1016/j.apsusc.2008.04.003>.
2. Liu H X, Xu Q, Wang C Q, and Zhang X W, *J Alloys Compd* **621** (2015) 357. <https://doi.org/10.1016/j.jallcom.2014.10.030>.
3. Kong W C, Li K M, and Hu J, *Opt Laser Technol* **142** (2021) 107214. <https://doi.org/10.1016/j.optlastec.2021.107214>.
4. Sharma S P, Dwivedi D K, and Jain P K, *Wear* **267** (2009) 853. <https://doi.org/10.1016/j.wear.2008.12.029>.
5. Guo C, Chen J M, Zhou J S, Zhao J R, Wang L Q, Yu Y J, and Zhou H D, *Surf Coat Technol* **206** (2012) 2064. <https://doi.org/10.1016/j.surfcoat.2011.06.005>.
6. Ravichandran K S, *Acta Metall Mater* **42** (1994) 143. [https://doi.org/10.1016/0956-7151\(94\)90057-4](https://doi.org/10.1016/0956-7151(94)90057-4).
7. Wu P, Du H M, Chen X L, Li Z Q, Bai H L, and Jiang E Y, *Wear* **257** (2004) 142. <https://doi.org/10.1016/j.wear.2003.10.019>.
8. Farahmand P, and Kovacevic R, *Surf Coat Technol* **276** (2015) 121. <https://doi.org/10.1016/j.surfcoat.2015.06.039>.
9. Zhao N, Tao L, Guo H, and Zhang M Q, *Rare Met Mater Eng* **46** (2017) 2092. <https://doi.org/10.3788/AL20103003.0173>.
10. Zhao W, and Kong D J, *Appl Surf Sci* **481** (2019) 161. <https://doi.org/10.1016/j.apsusc.2019.03.047>.
11. Lu M Y, Mead J, Wu Y Q, Russell H, and Huang H, *Mater Charact* **120** (2016) 337. <https://doi.org/10.1016/j.matchar.2016.09.020>.
12. Liu T Z, Chang M, Cheng X D, Zeng X, Shao H, and Liu F S, *Surf Coat Technol* **383** (2020) 125232. <https://doi.org/10.1016/j.surfcoat.2019.125232>.
13. Kang X Y, Nan Y, He Y H, Zhang M M, Yan Y, and Liu Y, *Ceram Int* **47** (2021) 19934. <https://doi.org/10.1016/j.ceramint.2021.03.328>.
14. Kong W C, Li K M, and Hu J, *Int J Hydrog Energy* **47** (2022) 6911. <https://doi.org/10.1016/j.ijhydene.2021.12.039>

15. Zhang M Y, Li M, Chi J, Wang S F, Yang S, Yang J, and Wei Y J, *Surf Coat Technol* **374** (2019) 645. <https://doi.org/10.1016/j.surfcoat.2019.06.066>.
16. Liu J S, and Shi Y, *Surf Coat Technol* **412** (2021) 127044. <https://doi.org/10.1016/j.surfcoat.2021.127044>.
17. Wang X, Rong J, Yao Y H, Zhang Y N, Zhong Y, Feng J, Yu X H, and Zhan Z L, *J Alloys Compd* **753** (2018) 688. <https://doi.org/10.1016/j.jallcom.2018.04.269>.
18. So H, Yu D S, and Chuang C Y, *Wear* **253** (2002) 1004. [https://doi.org/10.1016/S0043-1648\(02\)00230-2](https://doi.org/10.1016/S0043-1648(02)00230-2).
19. Kong W C, Li K M, and Hu J, *Opt Laser Technol*, **142** (2021) 107214. <https://doi.org/10.1016/j.optlastec.2021.107214>.
20. Huang C M, Zou B, Guo P, Liu Y N, Huang C Z, and Wang J, *Int J Refract Met Hard Mater* **59** (2016) 40. <https://doi.org/10.1016/j.ijrmhm.2016.05.007>.
21. Zhou J L, and Kong D J, *Surf Coat Technol* **408** (2021) 126816. <https://doi.org/10.1016/j.surfcoat.2020.126816>.

**Publisher's Note** Springer Nature remains neutral with regard to jurisdictional claims in published maps and institutional affiliations.